

Coupled cluster calculations provide a one-to-one mapping between calculated and observed transition energies in the electronic absorption spectrum of zinc phthalocyanine

A. J. Wallace, B. E. Williamson and D. L. Crittenden*

December 5, 2016

Abstract

All transitions in the experimentally designated and numbered Q, B and N bands (< 4.8 eV) of the electronic absorption spectrum of zinc phthalocyanine (ZnPc) are assigned on the basis of one-to-one agreement between calculated and experimentally observed transition energies and oscillator strengths. Each band in this range of the spectrum represents a ligand-based transition that originates from a combination of occupied orbitals and terminates in the lowest unoccupied molecular orbital (LUMO, $6e_g(\pi)$). Transition energies in the L and C regions (4.8 - 6.5 eV) are harder to capture quantitatively, due to the partial Rydberg character of some of the excited states, and so are tentatively assigned here. Most transitions in this range correspond to excitations from the HOMO or lower-energy orbitals to π orbitals above the LUMO.

*Department of Chemistry, University of Canterbury, Christchurch, New Zealand

INTRODUCTION

Metallophthalocyanines (MPcs, Figure 1a) are structurally similar to metalloporphyrinoids (Figure 1b), the chemical building blocks at the heart of important biological processes such as photosynthesis and respiration.¹ They share a range of optical and electronic properties with porphyrins, including high molar absorptivities, chemically tunable electronic energy levels, and excited states that are accessible through absorption of visible and ultra-violet light.^{2,3} However, their higher thermal stabilities and ease of synthesis make MPcs more chemically and technologically useful in many respects than their porphyrin analogues.⁴

Because of their optical properties, MPcs and their derivatives have long been exploited as dyes, and they currently account for 25% of worldwide organic pigment production.⁵ More recently, their electronic properties have been harnessed in more technologically advanced applications such as organic light-emitting diodes,⁶⁻⁸ organic photovoltaic materials^{7,9-13}, photo-sensitizing agents for anti-cancer photodynamic therapy¹⁴⁻¹⁷, and as MRI contrast agents¹⁸.

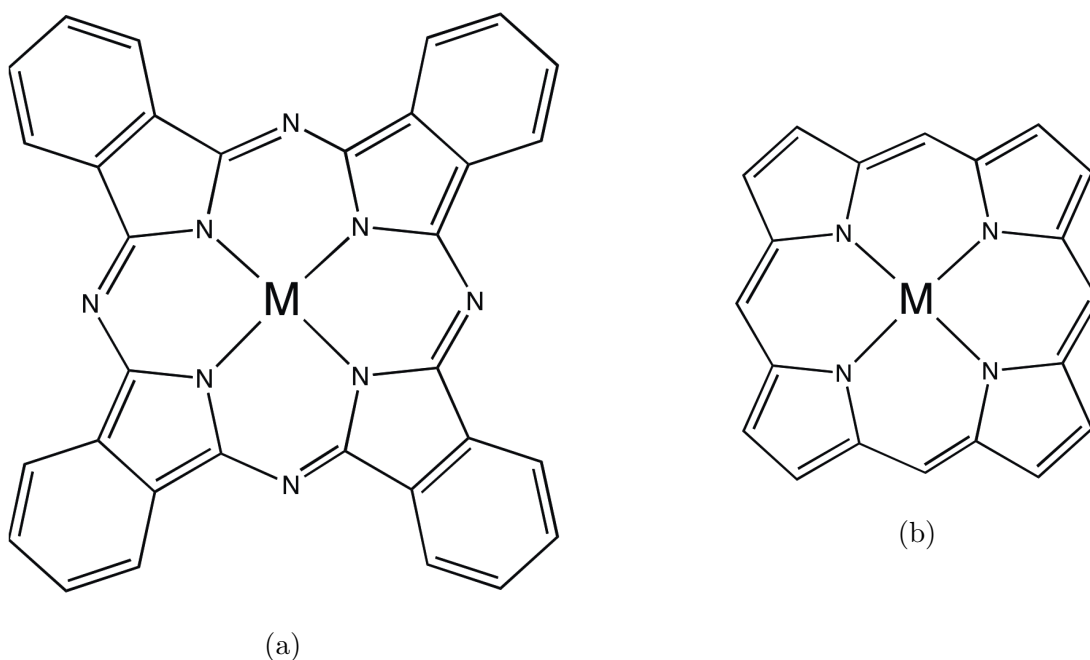


Figure 1: (a) Metallophthalocyanine and (b) metalloporphyrin molecular structures.

The demonstrated practical utility of MPcs⁵ has motivated extensive experimental and computational studies aiming to relate molecular properties and electronic structure.^{19–67}

Spectroscopically, the late first-row transition metal (Co, Ni, Cu, Zn)^{33,56} and alkali earth (Mg)⁴⁶ phthalocyanines are very similar, with practically superposable electronic absorption spectra dominated by ligand-based transitions, generally assigned as $\pi \rightarrow \pi^*$. By way of example, the ZnPc spectrum²⁴ is illustrated in Figure 2.

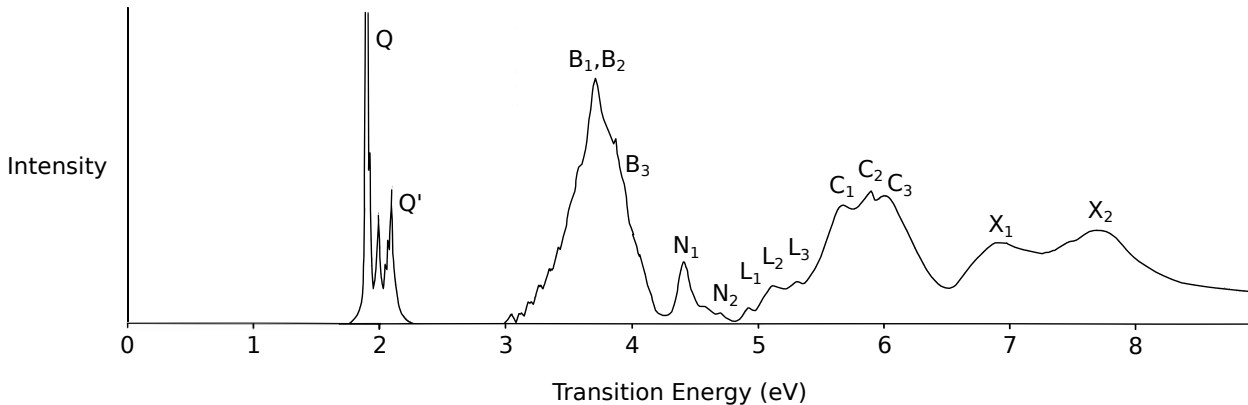


Figure 2: Electronic excitation spectrum of ZnPc in an argon matrix, adapted from VanCott *et al.*²⁴

The spectra of MnPc and FePc are quite different from that in Figure 2, with additional transitions observed below 2 eV.^{33,56} These transitions involve metal d orbitals with similar energies to the HOMO and LUMO of the ligand, significantly complicating the ground- and excited-state electronic structure of these systems. To avoid this additional complexity, previous theoretical and computational studies have largely focussed on modelling the simpler cases.

Taking ZnPc as a prototypical example, Gouterman *et al.* had early success assigning the Q band and partially characterizing the B band, using a simple four-electron, four-orbital configuration-interaction model, with ligand π orbitals and orbital energies obtained via Hückel theory.²⁰

Despite significant advances in computer hardware and quantum chemical software since

then, enabling an extensive series of semi-empirical (ZINDO)³⁵ and time-dependent density functional theory (TD-DFT)^{30,31,41,47,64,67,68} studies, the remaining transitions in the electronic absorption spectrum of ZnPc have eluded unambiguous characterization and assignment. Representative results from previous computational studies are presented, alongside experimental data collected in an argon matrix, in Table 1. In cases of near-duplication in methods and results, exact numerical values and spectral assignments are taken from the earliest study. ZINDO results³⁵ are omitted because they fail to identify any transitions with significant intensity in the B-band region.

The first B3LYP results, reported by Nguyen and Pachter,³⁰ have been reproduced almost exactly by subsequent studies using slightly different basis sets.^{35,64,68} More recently, the range-separated CAM-B3LYP and M11 functionals have been used by Theisen *et al.*,⁶⁷ but they do not report results for higher-energy transitions, nor do they comment on whether they observe the additional low-intensity, symmetry-allowed transitions in and around the Q- and B-band regions reported in other TD-DFT studies.^{30,31,47,64,68} The SAOP (statistical average of orbital potentials) functional, using a basis of Slater-type atomic orbitals, provides an alternative orbital-based approach for achieving range separation. The initial results reported by Ricciardi *et al.*³¹ have been verified in subsequent work.⁴⁷

From Table 1, not only are the predicted transition energies and intensities strongly functional-dependent, but there are significant discrepancies between the number of predicted and experimentally observed transitions in each region. Furthermore, different studies using similar methods propose alternative mappings between computational assignments and experimental data. Overall, the assignments of all transitions remain uncertain, except for Q and B₃, which are the lowest-energy computationally confirmed single-electron transitions of each of the two symmetry-allowed classes ($^1A_{1g} \rightarrow ^1E_u$ and $^1A_{1g} \rightarrow ^1A_{2u}$, respectively, in D_{4h}).

Previous computational studies on the closely related porphyrins have demonstrated that multi-determinant methods are essential for describing transitions originating from sets of near-degenerate ligand orbitals that are well separated from, but clustered together below, the HOMO.^{37,69–75} The inaccuracy of excited-state energies for large π systems calculated

Table 1: Experimental parameters and TD-DFT predictions for the ZnPc electronic absorption spectrum.

	Experiment - Ar matrix ²⁴		B3LYP/6-31G* ³⁰		M11/6-31G* ⁶⁷		SAOP/STO-TZ+pol ³¹	
Band Label	Transition Energy (eV)	Oscillator Strength (f/f_Q)	Transition Energy (eV)	Oscillator Strength (f/f_Q)	Transition Energy (eV)	Oscillator Strength (f/f_Q)	Transition Energy (eV)	Oscillator Strength (f/f_Q)
Q	1.89	1.00	2.09	1.00	1.88	1.00	1.96	1.00
Q'	2.08 [†]	0.08			2.10	0.84		
							2.87	0.04
							3.07	0.07
							3.14	0.41
							3.28	0.00
			3.37	0.02			3.34	0.06
B ₁	3.71	3.10	3.66	0.41	3.29	0.18	3.50	0.89
B ₂	3.74	0.10	3.74	0.78	3.82	0.17	3.81	1.57
			3.87	0.81				
B ₃	3.99 [†]	0.00	3.93	0.01			4.23	0.00
			3.96	0.28				
N ₁	4.41	0.28	4.34	0.46				
N ₂	4.70	0.05	-	-				
L ₁	4.88	0.03	5.14	0.03				
L ₂	5.10	0.24	5.19	0.24				
L ₃	5.33	0.25	5.36	0.07				
C ₁	5.62	0.74						
C ₂	5.92	0.06						
C ₃	6.00	2.13						
X ₁	6.89	1.46						
X ₂	7.67	2.03						

[†] Assigned as ${}^1A_{1g} \rightarrow {}^1A_{2u}$ transitions in D_{4h} symmetry. All others are ${}^1A_{1g} \rightarrow {}^1E_u$.

using TD-DFT has also been independently established by Grimme and Parac,⁷⁶ using linear condensed acenes as model systems.

The aim of the present work is to more robustly and extensively assign the electronic excitation spectrum of ZnPc, by using multi-determinant methods to accurately model its ground and excited electronic state energies and transition intensities.

METHODOLOGY

The molecular geometry is fixed in a D_{4h} conformation (coordinates available as Supporting Information) for both ground and excited state calculations. All electronic states and molecular orbitals are denoted using D_{4h} symmetry labels, with the latter in lower case. The ground state is ${}^1A_{1g}$ and the allowed electronic transitions are ${}^1A_{1g} \rightarrow {}^1E_u$ (polarized in the plane of the molecule) and ${}^1A_{1g} \rightarrow {}^1A_{2u}$ (polarized along the fourfold axis).

EOM-CCSD⁷⁷ and CR-EOM-CCSD(T)⁷⁸ calculations are performed using the GAMESS quantum chemical program package⁷⁹. The perturbative triples correction for the latter is evaluated by directly correcting the completely renormalized EOM-CCSD excitation energies using the IID variant of the triples correction defined by Kowalski and Piecuch, in a procedure denoted δ -CR-EOM-CCSD(T),IID.⁷⁸

Atomic orbitals (AOs) are initially expanded in the 3-21G basis,⁸⁰ because previous studies on porphins have shown that excitation energies for this type of extended conjugated π ring system are not particularly sensitive to the completeness of the AO basis.^{69,70} All molecular orbitals (MOs) constructed from this AO basis, except the chemical core, are included in the CCSD active space, while the CR-EOM-CCSD(T) active space comprises the 50 highest-energy occupied orbitals and 100 lowest energy unoccupied orbitals for excited states of 1E_u symmetry. The CR-EOM-CCSD(T) active space is extended to include the 75 highest-energy occupied orbitals for excited states of ${}^1A_{2u}$ symmetry, as these excited states are more sensitive to active space completeness.

Basis-set dependence is investigated both by expanding AOs in the more flexible 6-31G*

basis and by augmenting the 3-21G basis with additional ultra-diffuse Rydberg functions at the centre of mass (exponents available as Supporting Information). To offset the increased computational cost, the EOM-CCSD active space is truncated to include only 167 virtual MOs, in addition to the non-core occupied MOs. For reference, EOM-CCSD/3-21G calculations are also run in an equivalent active space.

Maintaining computational affordability is the primary consideration in setting active space truncation criteria, as required when either increasing the complexity of the method from CCSD to CCSD(T) or the size of the basis set from 3-21G to 6-31G*. We have chosen active spaces to be as large as possible within computational resourcing constraints.

RESULTS AND DISCUSSION

Benchmarking

Transition energies calculated at different levels of theory are presented in Table 2.

Benchmarking - electronic structure model

Comparing the CR-EOM-CCSD(T)/3-21G and EOM-CCSD/3-21G transition energies reported in Table 2, it is clear that EOM-CCSD systematically overestimates transition energies. This is most likely due to the inability of the coupled cluster wavefunction to completely compensate for ground-state orbital optimization bias. Destabilizing the EOM-CCSD/3-21G ground state by +0.48 eV or, equivalently, stabilizing each excited state by -0.48 eV, would account for the systematic bias in favour of the ground state, and bring EOM-CCSD transition energies into good agreement (< 0.15 eV difference) with their CR-EOM-CCSD(T) counterparts for all states up to and including ${}^1E_u(8)$.

As an aside, we note that it may not always be practical to perform CR-EOM-CCSD(T) calculations. In such cases, an empirical offset could be derived by aligning the first calculated and experimentally observed transition energies. For ZnPc, this would equate to 0.53

Table 2: Transition energies calculated at different levels of theory; CR-EOM-CCSD(T)/3-21G with a truncated active space, EOM-CCSD/3-21G in a full active space, and EOM-CCSD in a range of different basis sets with a truncated active space.

Transition Symmetry Label	CR-EOM- CCSD(T)/ 3-21G ^a	EOM- CCSD/ 3-21G ^b	EOM - CCSD/ 3-21G ^c	EOM- CCSD/ 6-31G ^{*c}	EOM - CCSD/ 3-21G+Ryd ^c
¹ A _{1g} → ¹ E _u (1)	2.09	2.42	2.49	2.39	2.45
¹ A _{1g} → ¹ E _u (2)	3.93	4.34	4.31	4.29	4.29
¹ A _{1g} → ¹ E _u (3)	4.07	4.52	4.53	4.45	4.47
¹ A _{1g} → ¹ A _{2u} (1) [†]	<i>4.11</i>	<i>4.57</i>	<i>4.6</i>	<i>4.86</i>	<i>4.7</i>
¹ A _{1g} → ¹ E _u (4)	4.38	4.82	4.85	4.71	4.8
¹ A _{1g} → ¹ E _u (5)	4.47	5.06	5.09	4.94	5.04
¹ A _{1g} → ¹ E _u (6)	4.72	5.3	5.36	5.02	5.31
¹ A _{1g} → ¹ E _u (7)	5.22	5.7	5.77	5.58	5.72
¹ A _{1g} → ¹ E _u (8)	5.66	6.16	6.2	6	6.16
¹ A _{1g} → ¹ A _{2u} (2) [†]	<i>5.82</i>	<i>6.85</i>	<i>6.23</i>	<i>6.44</i>	<i>5.86</i>
¹ A _{1g} → ¹ E _u (9)	6.16	6.95	6.97	6.71	6.54
¹ A _{1g} → ¹ E _u (10)	6.43	7	7.01	6.83	<i>d</i>

^a Active space includes 50/75[†] highest energy occupied MOs and 100 lowest energy virtuals

^b Active space includes all MOs, except the chemical core

^c Active space includes all non-core occupied MOs and 167 lowest energy virtuals

^d Could not obtain converged solution for this state

eV. Reassuringly, the computationally- and experimentally-derived corrections are similar.

The agreement between empirically corrected EOM-CCSD/3-21G transition energies and their CR-EOM-CCSD(T) counterparts deteriorates for transitions to higher excited states, especially ${}^1A_{2u}(2)$ and ${}^1E_u(9)$. This implies that these different electronic structure models have different sensitivities to basis set incompleteness and active space truncation.

Benchmarking - basis set and active space incompleteness

Overall, the results presented in Table 2 support previous observations that excitation energies for porphyrinoid ring systems are not particularly sensitive to the completeness of the atomic orbital basis.^{69,70} Increasing the basis set from 3-21G to 6-31G* changes the transition energies by 0.18 eV, on average, stabilizing the 1E_u excited states and destabilizing the ${}^1A_{2u}$ excited states in approximately equal measure.

Caution is required when interpreting these results purely in terms of basis set incompleteness effects, because although these EOM-CCSD calculations were carried out equivalently sized active spaces, there is no guarantee that that active space composition is the same. It is likely that the 6-31G* active space contains less virtual orbitals of ${}^1A_{2u}$ symmetry, and more of 1E_u , compared to the equivalent 3-21G active space. The truncated 3-21G active space has, in turn, been benchmarked against an untruncated 3-21G active space, giving very similar results – within 0.07 eV – for all transition energies except ${}^1A_{1g} \rightarrow {}^1A_{2u}(2)$.

The ${}^1A_{1g} \rightarrow {}^1A_{2u}(2)$ transition energy is particularly sensitive to *both* atomic orbital basis completeness and coupled-cluster active space composition, and these effects cannot be clearly deconvoluted. From the results presented Table 2, we can conclude only that any particular calculated ${}^1A_{1g} \rightarrow {}^1A_{2u}(2)$ transition energy may be in error up to 1 eV.

The computationally intensive nature of equations-of-motion coupled cluster calculations means that there is no simple way to resolve the uneasy tension between including more atomic orbitals in the underlying basis set, or including a more complete set of molecular orbitals in the coupled cluster active space. However, because the basis set incompleteness

error is systematic and relatively small, we have chosen to employ the 3-21G basis set in order to use the most complete active space in the coupled cluster calculations.

Benchmarking - Rydberg functions

It is substantially easier to assess the limitations of the 3-21G basis in describing Rydberg excited states, by simply augmenting the atomic orbital basis set with additional ultra-diffuse “Rydberg” functions at the molecule’s centre of mass. These additional orbitals do not change the composition of the active space, because they are substantially higher in energy than the valence orbitals and so fall into the set of orbitals excluded from coupled cluster excitations. Therefore, they simply provide the flexibility required for the existing active space orbitals to expand into the Rydberg region.

Results from restricted active space EOM-CCSD/3-21G calculations both with and without Rydberg functions (Table 2) clearly show that only the three highest-energy transitions are to excited states with substantial Rydberg character.

Assignment of experimental spectrum

Assignments for all transitions, except Q’, in the Q, B, N, L and C regions of the experimental spectrum, are presented in Table 3.

Assignment - Q, B and N regions

Assignments of transitions within the Q, B and N regions are based upon close correspondence between calculated and experimentally observed transition energies, and can be made with a high degree of confidence because excited state energies are relatively insensitive to basis set incompleteness in these regions. These assignments are further supported by qualitative agreement between calculated and observed transition intensities, reported as normalized oscillator strengths in Table 3.

Individual bands within the Q, B and N regions correspond to transitions that originate from

Table 3: CR-EOM-CCSD(T)/3-21G predictions of electronic band origins and EOM-CCSD/3-21G normalized oscillator strengths and principal excitations.

Band Label	Experiment Ar matrix		CR-EOM- CCSD(T)/ 3-21G	EOM-CCSD/3-21G	
	Transition Energy (eV)	Oscillator Strength (f/f_Q)	Transition Energy (eV)	Oscillator Strength (f/f_Q)	Principal excitations*
Q	1.89	1.00	2.09	1.00	$2a_{1u}(\pi) \rightarrow 6e_g(\pi)$
Q'	2.08 [†]	0.08			
B ₁	3.71	3.10	3.93	2.61	$\{3a_{2u}(\pi), 4a_{2u}(\pi)\} \rightarrow 6e_g(\pi)$
B ₂	3.74	0.10	4.07	0.54	$\{2b_{1u}(\pi), 4a_{2u}(\pi)\} \rightarrow 6e_g(\pi)$
B ₃	3.99 [†]	0.00	4.11 [†]	0.02	$2e_u(\sigma) \rightarrow 6e_g(\pi)$
N ₁	4.41	0.28	4.38	0.98	$\{4a_{2u}(\pi), 3b_{2u}(\pi)\} \rightarrow 6e_g(\pi)$
N ₂	4.70	0.05	4.47	0.37	$\{3a_{2u}(\pi), 3b_{2u}(\pi)\} \rightarrow 6e_g(\pi)$
L ₁	4.88	0.03	4.72	0.24	$2a_{1u}(\pi) \rightarrow 7e_g(\pi)$
L ₂	5.10	0.24	5.22	0.44	$\{3b_{2u}(\pi), 1a_{1u}(\pi)\} \rightarrow 6e_g(\pi)$
L ₃	5.33	0.25	5.66	0.27	$1a_{1u}(\pi) \rightarrow 6e_g(\pi), 2a_{1u}(\pi) \rightarrow 8e_g(\pi)$
C ₁	5.62	0.74	5.82 ^{†,‡}	0.02	$2b_{1g}(\sigma) \rightarrow 4b_{2u}(\pi)$
C ₂	5.92	0.06	6.16 [‡]	0.12	$5e_g(\pi) \rightarrow 3b_{1u}(\pi)$
C ₃	6.00	2.13	6.43 [‡]	1.66	$2a_{1u}(\pi) \rightarrow 7e_g(\pi)$
X ₁	6.89	1.46			
X ₂	7.67	2.03			

* $2a_{1u}(\pi)$ = HOMO, $6e_g(\pi)$ = LUMO, see Figure 3

[†] assigned as ${}^1A_{1g} \rightarrow {}^1A_{2u}$ transitions, all others assigned as ${}^1A_{1g} \rightarrow {}^1E_u$.

[‡] partial Rydberg character not accounted for here.

orbitals at or below the HOMO and terminate in the LUMO, as per the dominant excitation amplitudes (coefficients > 0.25) listed in Table 3 and illustrated in Figure 3, based upon the Hartree-Fock molecular orbitals shown in Figure 4. All are ligand-based $\pi \rightarrow \pi$ transitions of ${}^1A_{1g} \rightarrow {}^1E_u$ symmetry, except for B_3 , which involves $\sigma \rightarrow \pi$ excitations and is of symmetry ${}^1A_{1g} \rightarrow {}^1A_{2u}$.

In agreement with previous computational studies,^{30,31,35,47,64,67} the Q band can be described essentially as a single-electron $2a_{1u}(\pi) \rightarrow 6e_g(\pi)$ excitation from the HOMO and the LUMO. Both the HOMO and LUMO are energetically well separated from other orbitals, so the excited state is predominantly single-reference. The B_3 band at 3.99 eV, previously assigned as a ${}^1A_{1g} \rightarrow {}^1A_{2u}$ transition on the basis of experimental data,²⁴ is confirmed as the lowest energy ${}^1A_{1g} \rightarrow {}^1A_{2u}$ transition of the system.

All other excited states within 4.8 eV of the ground state have significant multi-determinant character, involving excitations to the LUMO originating from a set of occupied π orbitals clustered together at energies significantly lower than the HOMO. There is little to no correspondence between the state assignments provided here and results from previous DFT studies.^{30,31,35,47,64,67} Only in this study does the number of predicted transitions within each region match experimental observations.

Tentative Assignment - L and C regions

Of all bands in the L and C regions, only the C_3 band can be unambiguously assigned, based upon transition intensity data. As shown in Table 3, it is the second most intense transition in the spectrum, both computationally and experimentally. The fact that the transition energy is overestimated by 0.43 eV is explained by the inability of the EOM-CCSD(T)/3-21G model to completely capture the Rydberg character of this excited state.

The remaining transitions cannot be unambiguously assigned, due to uncertainties in calculated transition energies and oscillator strengths. The most straightforward assignment simply preserves the EOM-CCSD(T)/3-21G energy ordering, as shown in Table 3.

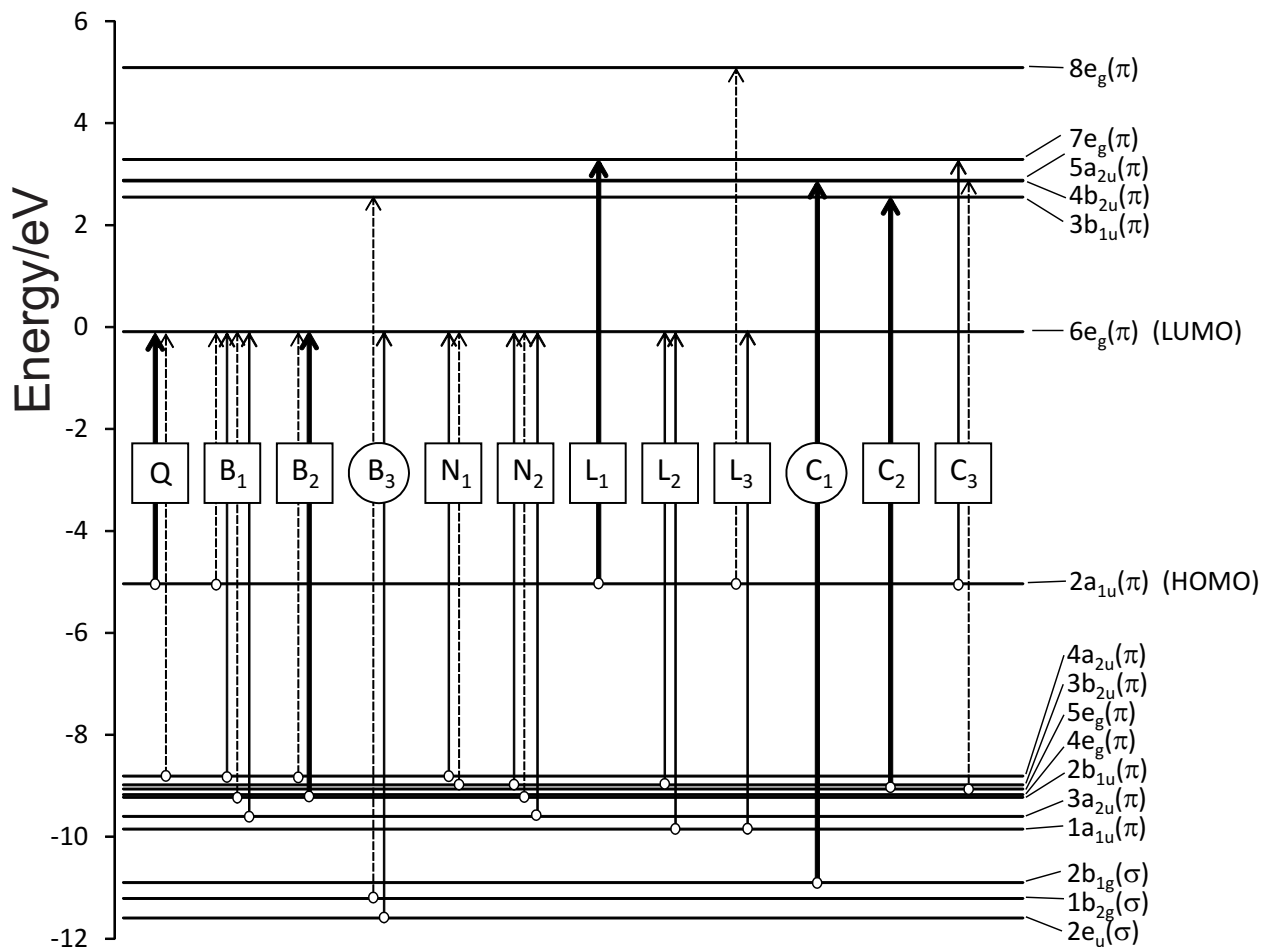


Figure 3: Energy-level diagram illustrating dominant excitations in the formation of excited electronic states of ZnPc, according to EOM-CCSD/3-21G calculations based upon HF/3-21G reference orbitals. The orbital labels and energies refer to the Hartree-Fock MOs illustrated in Figure 4. Excitations with coefficients > 0.45 are indicated in bold, between 0.30 and 0.45 using unbroken lines, and between 0.2 and 0.3 using dashed lines. ${}^1A_{1g} \rightarrow {}^1E_u$ transitions have square labels, while ${}^1A_{1g} \rightarrow {}^1A_{2u}$ are circular.

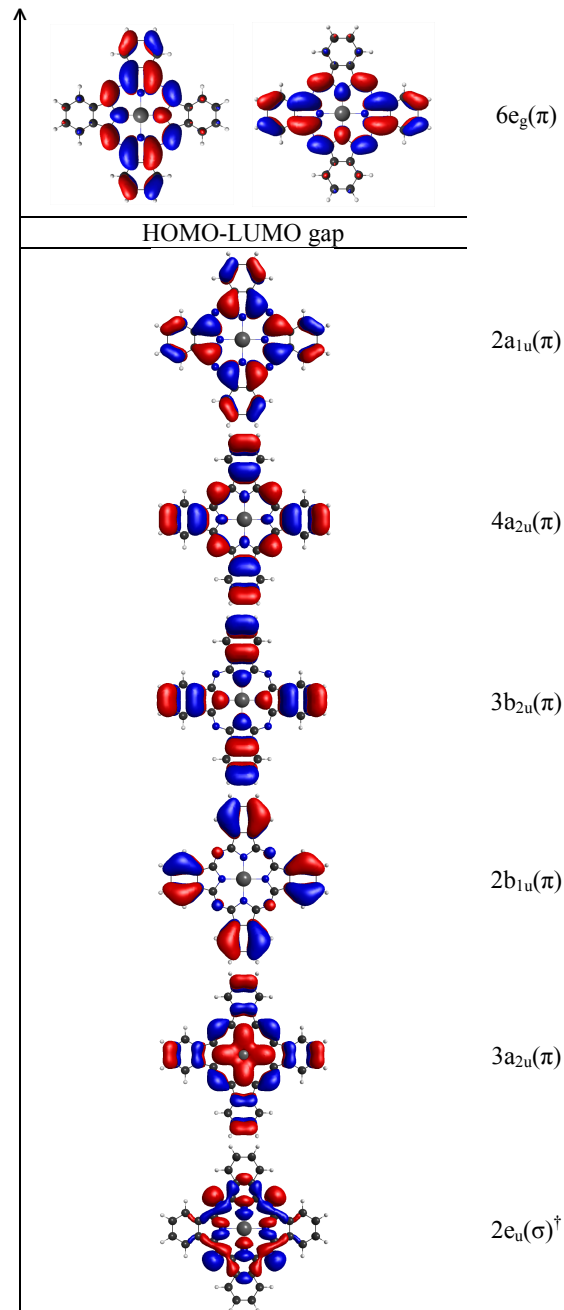


Figure 4: Dominant partially-occupied Hartree-Fock molecular orbitals that form the basis of EOM-CCSD excited states within the experimentally designated Q, B and N regions of the electronic absorption spectrum. Orbitals increase in energy up the page. The $6e_g(\pi)$ orbitals form the doubly-degenerate LUMO and the $2a_{1u}(\pi)$ orbital is the HOMO.

However, we have previously established that the $\sigma \rightarrow \pi$ transition of symmetry ${}^1A_{1g} \rightarrow {}^1A_{2u}$ denoted C_1 in Table 3, may be overestimated by up to 1 eV. Taking this uncertainty into account, an alternative assignment may be arrived at by matching patterns of predicted and observed transition intensities, while preserving the ordering of states within each symmetry-allowed class. In this case, the $\sigma \rightarrow \pi$ transition would correspond to band L_1 , with the assignments for all other transitions offset accordingly ($L_1 \rightarrow L_2$, etc).

Despite the ambiguity in transition assignments, this is the first computational study to yield the correct number of transitions within each experimentally-designated spectral region. In effect, the C_3 assignment book-ends the L and C regions, ensuring a one-to-one mapping between calculated and observed transitions. It is also the first time that detailed assignments have been proposed for transitions within the C region.

With the exception of the transition we have denoted C_1 , all remaining transitions in the L and C regions may be categorised as $\pi \rightarrow \pi$ transitions of symmetry ${}^1A_{1g} \rightarrow {}^1E_u$, in accordance with experimental observations.²⁴ Further, all transitions in the C band involve excitations from orbitals below the HOMO to orbitals above the LUMO (Figure 3 and Table 3), and demonstrate a substantial degree of Rydberg character (Table 2).

We do not attempt to model transitions in the X band, which are probably of predominantly Rydberg character.²⁴

Discussion - the Q' band

The origin of the Q' band has long been the source of significant speculation in the literature. Magnetic circular dichroism data indicate that this region contains both a vibronic side-band of the Q transition *and* an additional electronic transition. However, recent computational results suggest that Q' is well-modelled exclusively as a vibronic side-band of Q.⁶⁷

We have not identified any possible spin-singlet excited states, symmetry-forbidden or otherwise, in the correct energy region. Therefore, in agreement with Theisen *et al*,⁶⁷ we can rule out the hypothesis that Q' corresponds to a orbitally symmetry-forbidden transition

‘borrowing’ intensity from a symmetry-allowed transition purely through vibronic coupling.

However, it remains a possibility that an additional electronic transition arises due to intersection between the singlet Q state and the lowest excited triplet state. Conclusively ruling such a transition in, or out, would require consideration of both spin-orbit and vibronic coupling effects.

CONCLUSIONS

High level *ab initio* methods are required to accurately model the electronic absorption spectrum of ZnPc. Using δ -CR-EOM-CCSD(T)-IID/3-21G, we have unambiguously assigned all transitions, except Q’, in the Q, B and N regions of the spectrum, and have tentatively assigned all bands in the L and C regions. Importantly, and unlike previous DFT studies,^{30,31,35,47,64,67} we demonstrate a one-to-one correspondence between number of predicted and observed transitions in each region, along with qualitatively correct intensities. To obtain quantitatively correct results, it will be necessary to both increase the completeness of the atomic orbital basis *and* concurrently increase the extent of the coupled cluster active space. This remains a daunting computational challenge.

The assignments provided herein for ZnPc will also apply to other metal phthalocyanines with the same spectroscopic signature; those whose metal *d* orbitals are well separated energetically from the ligand HOMO and LUMO. For MPcs with metal *d* orbitals that have energies near the HOMO-LUMO gap, the multireference problem becomes acute and is likely to require even more sophisticated electronic structure models.

ACKNOWLEDGMENTS

The authors acknowledge the contribution of NeSI high-performance computing facilities to the results of this research. New Zealand’s national facilities are provided by the NZ eScience Infrastructure and funded jointly by NeSI’s collaborator institutions and through the Ministry of Business, Innovation & Employment’s Research Infrastructure programme. URL <https://www.nesi.org.nz>. This work was also supported by the Marsden Fund Council

from Government funding, administered by the Royal Society of New Zealand.

SUPPORTING INFORMATION

Additional Supporting Information that may be found in the online version of this article includes the ZnPc geometry, Rydberg basis function exponents, and a diagram including the complete set of orbitals involved in all assigned transitions.

References

1. Milgram, L. R. *The Colours of Life. An Introduction to the Chemistry of Porphyrins and Related Compounds.*; Oxford University Press: Oxford, 1997.
2. Armstrong, N. R. *J. Porph. Phthalo.* **2000**, *4*, 414–417.
3. Nyokong, T. *Coord. Chem. Rev.* **2007**, *251*, 1707–1722.
4. Gregory, P. *J. Porph. Phthalo.* **2000**, *4*, 432–437.
5. Löbbert, G. *Ullmann's Encyclopedia of Industrial Chemistry*; Wiley-VCH Verlag GmbH & Co. KGaA, 2000.
6. VanSlyke, S. A.; Chen, C. H.; Tang, C. W. *App. Phys. Lett.* **1996**, *69*, 2160–2162.
7. Armstrong, N. R.; Wang, W.; Alloway, D. M.; Placencia, D.; Ratcliff, E.; Brumbach, M. *Macromol. Rap. Comm.* **2009**, *30*, 717–731.
8. Li, L.; Guan, M.; Cao, G.; Li, Y.; Zeng, Y. *Displays* **2012**, *33*, 17–20.
9. Rand, B. P.; Genoe, J.; Heremans, P.; Poortmans, J. *Prog. Photovolt.* **2007**, *15*, 659–676.
10. Kushto, G. P.; Maekinen, A. J.; Lane, P. A. *IEEE J. Sel. Top. Quant. Elec.* **2010**, *16*, 1552–1559.
11. Taffa, D. H.; Kathiresan, M.; Arnold, T.; Walder, L.; Erbacher, M.; Bauer, D.; Montforts, F.-P.; Nordmann, J.; Haase, M. *J. Photochem. Photobiol. A* **2010**, *216*, 35–43.
12. Walter, M. G.; Rudine, A. B.; Wamser, C. C. *J. Porph. Phthalo.* **2010**, *14*, 759–792.
13. Chawla, P.; Tripathi, M. *Int. J. Energy Res.* **2015**, *39*, 1579–1596.
14. Bonnett, R. *Chem. Soc. Rev.* **1995**, *24*, 19–33.
15. Banfi, S.; Caruso, E.; Buccafurni, L.; Ravizza, R.; Gariboldi, M.; Monti, E. *J. Organomet. Chem.* **2007**, *692*, 1269–1276.

16. Moreira, L. M.; dos Santos, F. V.; Lyon, J. P.; Maftoum-Costa, M.; Pacheco-Soares, C.; da Silva, N. S. *Aust. J. Chem.* **2008**, *61*, 741–754.
17. Ogbodu, R. O.; Nyokong, T. *Spectrochim. Acta A* **2015**, *151*, 174–183.
18. Saini, S. K.; Jena, A.; Dey, J.; Sharma, A. K.; Singh, R. *Mag. Res. Imaging* **1995**, *13*, 985–990.
19. Lucia, E. A.; Verderam, F. D. *J. Chem. Phys.* **1968**, *48*, 2674–2681.
20. Edwards, L.; Gouterman, M. *J. Mol. Spec.* **1970**, *33*, 292–310.
21. Henriksson, A.; Roos, B.; Sundbom, M. *Theoret. Chim. Acta* **1972**, *27*, 303–313.
22. Edwards, L.; Gouterman, M.; Rose, C. B. *J. Am. Chem. Soc.* **1976**, *98*, 7638–7641.
23. Davidson, A. T. *J. Chem. Phys.* **1982**, *77*, 168–172.
24. VanCott, T. C.; Rose, J. L.; Misener, G. C.; Williamson, B. E.; Schrimpf, A. E.; Boyle, M. E.; Schatz, P. N. *J. Phys. Chem.* **1989**, *93*, 2999–3011.
25. Williamson, B. E.; VanCott, T. C.; Boyle, M. E.; Misener, G. C.; Stillman, M. J.; Schatz, P. N. *J. Am. Chem. Soc.* **1992**, *114*, 2412–2419.
26. Mack, J.; Stillman, M. J. *J. Phys. Chem.* **1995**, *99*, 7935–7945.
27. Plows, F. L.; Jones, A. C. *J. Mol. Spec.* **1999**, *194*, 163–170.
28. Liao, M. S.; Scheiner, S. *J. Chem. Phys.* **2001**, *114*, 9780–9791.
29. Mack, J.; Stillman, M. J. *Inorg. Chem.* **2001**, *40*, 812–814.
30. Nguyen, K. A.; Pachter, R. *J. Chem. Phys.* **2001**, *114*, 10757–10767.
31. Ricciardi, G.; Rosa, A.; Baerends, E. J. *J. Phys. Chem. A* **2001**, *105*, 5242–5254.
32. Rosa, A.; Ricciardi, G.; Baerends, E. J.; van Gisbergen, S. J. A. *J. Phys. Chem. A* **2001**, *105*, 3311–3327.

33. Yoshida, H.; Tsutsumi, K.; Sato, N. *J. Elec. Spec.* **2001**, *121*, 83 – 91.
34. Liao, M. S.; Scheiner, S. *J. Comp. Chem.* **2002**, *23*, 1391–1403.
35. Zhou, X.; Ren, A. M.; Feng, J. K.; Liu, X. J. *Can. J. Chem.* **2004**, *82*, 19–26.
36. Gantchev, T. G.; van Lier, J. E.; Hunting, D. J. *Rad. Phys. Chem.* **2005**, *72*, 367–379.
37. Hasegawa, J. Y.; Takata, K.; Miyahara, T.; Neya, S.; Frisch, M. J.; Nakatsuji, H. *J. Phys. Chem. A* **2005**, *109*, 3187–3200.
38. Liao, M. S.; Watts, J. D.; Huang, M. J. *Inorg. Chem.* **2005**, *44*, 1941–1949.
39. Seoudi, R.; El-Bahy, G. S.; El Sayed, Z. A. *Optic. Mat.* **2006**, *29*, 304–312.
40. Calzolari, A.; Ferretti, A.; Nardelli, M. B. *Nanotech.* **2007**, *18*, 424013.
41. Nemykin, V. N.; Hadt, R. G.; Belosludov, R. V.; Mizuseki, H.; Kawazoe, Y. *J. Phys. Chem. A* **2007**, *111*, 12901–12913.
42. Peralta, G. A.; Seth, M.; Ziegler, T. *Inorg. Chem.* **2007**, *46*, 9111–9125.
43. Pei, L.; Zhang, J.; Kong, W. *J. Chem. Phys.* **2007**, *127*, 174308.
44. Kuzmitsky, V. A.; Volkovich, D. I. *J. App. Spec.* **2008**, *75*, 27–35.
45. Marom, N.; Hod, O.; Scuseria, G. E.; Kronik, L. *J. Chem. Phys.* **2008**, *128*, 164107.
46. Peltekis, N.; Holland, B. N.; Krishnamurthy, S.; McGovern, I. T.; Poolton, N. R.; Patel, S.; McGuinness, C. *J. Am. Chem. Soc.* **2008**, *130*, 13008–13012.
47. Peralta, G. A.; Seth, M.; Zhekova, H.; Ziegler, T. *Inorg. Chem.* **2008**, *47*, 4185–4198.
48. Govind, N.; Valiev, M.; Jensen, L.; Kowalski, K. *J. Phys. Chem. A* **2009**, *113*, 6041–6043.
49. Grobosch, M.; Aristov, V. Y.; Molodtsova, O. V.; Schmidt, C.; Doyle, B. P.; Nannarone, S.; Knupfer, M. *J. Phys. Chem. C* **2009**, *113*, 13219–13222.

50. Marom, N.; Kronik, L. *App. Phys. A* **2009**, *95*, 159–163.
51. Marom, N.; Kronik, L. *App. Phys. A* **2009**, *95*, 165–172.
52. Maslyuk, V. V.; Aristov, V. Y.; Molodtsova, O. V.; Vyalikh, D. V.; Zhilin, V. M.; Ossipyan, Y. A.; Bredow, T.; Mertig, I.; Knupfer, M. *App. Phys. A* **2009**, *94*, 485–489.
53. Kraus, R.; Grobosch, M.; Knupfer, M. *Chem. Phys. Lett.* **2009**, *469*, 121–124.
54. Kuz'min, M. D.; Hayn, R.; Oison, V. *Phys. Rev. B* **2009**, *79*, 024413.
55. Bruder, I.; Schoeneboom, J.; Dinnebier, R.; Ojala, A.; Schaefer, S.; Sens, R.; Erk, P.; Weis, J. *Org. Elec.* **2010**, *11*, 377–387.
56. Grobosch, M.; Schmidt, C.; Kraus, R.; Knupfer, M. *Org. Elec.* **2010**, *11*, 1483–1488.
57. Roth, F.; Koenig, A.; Kraus, R.; Grobosch, M.; Kroll, T.; Knupfer, M. *Eur. Phys. J. B* **2010**, *74*, 339–344.
58. Grobosch, M.; Mahns, B.; Loose, C.; Friedrich, R.; Schmidt, C.; Kortus, J.; Knupfer, M. *Chem. Phys. Lett.* **2011**, *505*, 122–125.
59. Marom, N.; Ren, X.; Moussa, J. E.; Chelikowsky, J. R.; Kronik, L. *Phys. Rev. B* **2011**, *84*, 195143.
60. Stradi, D.; Diaz, C.; Martin, F.; Alcamí, M. *Theor. Chem. Acc.* **2011**, *128*, 497–503.
61. Kroll, T.; Kraus, R.; Schoenfelder, R.; Aristov, V. Y.; Molodtsova, O. V.; Hoffmann, P.; Knupfer, M. *J. Chem. Phys.* **2012**, *137*, 054306.
62. Guo, M.; He, R.; Dai, Y.; Shen, W.; Li, M.; Zhu, C.; Lin, S. H. *J. Chem. Phys.* **2012**, *136*, 144313.
63. Valiev, R. R.; Cherepanov, V. N.; Artyukhov, V. Y.; Sundholm, D. *Phys. Chem. Chem. Phys.* **2012**, *14*, 11508–11517.
64. Ueno, L. T.; Jayme, C. C.; Silva, L. R.; Pereira, E. B.; de Oliveira, S. M.; Machado, A. E. H. *J. Braz. Chem. Soc.* **2012**, *23*, 2237–2247.

65. Arillo-Flores, O. I.; Fadlallah, M. M.; Schuster, C.; Eckern, U.; Romero, A. H. *Phys. Rev. B* **2013**, *87*, 165115.
66. Yanagisawa, S.; Yasuda, T.; Inagaki, K.; Morikawa, Y.; Manseki, K.; Yanagida, S. *J. Phys. Chem. A* **2013**, *117*, 11246–11253.
67. Theisen, R. F.; Huang, L.; Fleetham, T.; Adams, J. B.; Li, J. *J. Chem. Phys.* **2015**, *142*, 094310.
68. Tussupbayev, S.; Govind, N.; Lopata, K.; Cramer, C. J. *Journal of Chemical Theory and Computation* **2015**, *11*, 1102–1109.
69. Merchan, M.; Orti, E.; Roos, B. O. *Chem. Phys. Lett.* **1994**, *221*, 136–144.
70. Serrano-Andres, L.; Merchan, M.; Rubio, M.; Roos, B. O. *Chem. Phys. Lett.* **1998**, *295*, 195–203.
71. Gwaltney, S. R.; Bartlett, R. J. *J. Chem. Phys.* **1998**, *108*, 6790–6798.
72. Rubio, M.; Roos, B. O.; Serrano-Andres, L.; Merchan, M. *J. Chem. Phys.* **1999**, *110*, 7202–7209.
73. Parusel, A. B. J.; Grimme, S. *J. Porph. Phthal.* **2001**, *5*, 225–232.
74. Kowalski, K.; Krishnamoorthy, S.; Villa, O.; Hammond, J. R.; Govind, N. *J. Chem. Phys.* **2010**, *132*, 154103.
75. Kowalski, K.; Olson, R. M.; Krishnamoorthy, S.; Tipparaju, V.; Apra, E. *J. Chem. Theor. Comp.* **2011**, *7*, 2200–2208.
76. Grimme, S.; Parac, M. *ChemPhysChem* **2003**, *4*, 292–295.
77. Comeau, D. C.; Bartlett, R. J. *Chem. Phys. Lett.* **1993**, *207*, 414–423.
78. Kowalski, K.; Piecuch, P. *J. Chem. Phys.* **2004**, *120*, 1715–1738.

79. Schmidt, M. W.; Baldrige, K. K.; Boatz, J. A.; Elbert, S. T.; Gordon, M. S.; Jensen, J. H.; Koseki, S.; Matsunaga, N.; Nguyen, K. A.; Su, S. J.; Windus, T. L.; Dupuis, M.; Montgomery, J. A. *J. Comp. Chem.* **1993**, *14*, 1347–1363.
80. Binkley, J. S.; Pople, J. A.; Hehre, W. J. *J. Am. Chem. Soc.* **1980**, *102*, 939–947.